IET Generation, Transmission & Distribution

IET The Institution of Engineering and Technology WILEY

ORIGINAL RESEARCH

Optimal power flow-based reactive power control in smart distribution network using real-time cyber-physical co-simulation framework

Raju Wagle[1] | Pawan Sharma[1] | Charu Sharma[1] | Mohammad Amin[2] |
Jose Luis Rueda[3] | Francisco Gonzalez-Longatt[4]

[1]Department of Electrical Engineering, UiT The Arctic University of Norway, Narvik, Norway

[2]Department of Electric Power Engineering, NTNU, Trondheim, Norway

[3]Department of Electrical Sustainable Energy, Delft University of Technology, Delft, The Netherlands

[4]Center for Smart Grid, Department of Engineering, University of Exeter, Exeter, UK

Correspondence
Raju Wagle, Department of Electrical Engineering, UiT The Arctic University of Norway, Lodve Langesgate 2, 8514 Narvik, Norway.
Email: raju.wagle@uit.no

Abstract

Future distribution networks (DN) are subject to rapid load changes and high penetration of variable distributed energy resources (DER). Due to this, the DN operators face several operational challenges, especially voltage violations. Optimal power flow (OPF)-based reactive power control (RPC) from the smart converter (SC) is one of the viable solutions to address such violations. However, sufficient communication and monitoring infrastructures are not available for OPF-based RPC. With the development of the latest information communication technology in SC, cyber-physical co-simulation (CPCS) has been extensively used for real-time monitoring and control. Moreover, deploying OPF-based RPC using CPCS considering the controller design of SC for a realistic DN is still a big challenge. Hence, this paper aims to mitigate voltage violations by using OPF-based RPC in a real-time CPCS framework with multiple SCs in a realistic DN. The OPF-based RPC is achieved by performing the CPCS framework developed in this study. The CIGRE medium-voltage DN is considered as a test system. Real-time optimization and signal processing are achieved by Python-based programs using a model-based toolchain of a real-time DN solver and simulator. Real-time simulation studies showed that the proposed method is capable of handling uncertain voltage violations in real time.

1 | INTRODUCTION

Global awareness of carbon neutrality, increased energy demand, technological advancement in control strategies, and significant cost reduction have encouraged power system operators to incorporate more renewable energy-based distributed energy resources (DER) into the distribution network (DN) [1]. To run the DN with higher observability, controllability, and flexibility, the DNs are transitioning from conventional architecture to smart architecture [2]. DNs are now operated in the smart grid paradigm and hence are also renamed smart distribution networks (SDNs). In smart architecture, SDNs are equipped with smart meters, smart converters (SC) [3], intelligent electronic devices (IED), and advanced communication infrastructure. For smart operation, SDN requires a

more resilient, robust, and high-speed control and management system [4].

SDN poses many technical challenges with the high integration of DER and recent modernization in network operation [5, 6]. One significant challenge in SDN is maintaining an efficient and robust regulation of fluctuating node voltages [7, 8]. Generally, the DERs are connected to the SDN using SCs. The use of SCs as a quick response solution to regulate voltage using RPC can be a suitable choice [9, 10]. Furthermore, with the advancement of SC technology, most SCs have powerful communication and monitoring equipment [11]. Therefore, they can meet the requirement for smart operation in SDN without additional investments [12].

Reactive power control (RPC) of SCs can be achieved in several ways [13]. Provided adequate communication, control,

and monitoring infrastructure is available, optimal power flow (OPF)-based RPC is one of the most suitable solutions [14]. Optimal RPC and SDN management strategies should also consider moving away from traditional offline approaches and shifting towards real-time solutions to make the system more reliable, fast, and precise [15]. Although many researchers [16, 17] contribute to the development of autonomous systems to improve interaction, resiliency, effectiveness, and reliability, little attention is paid to real-time implementation. So far, only some smart grid functionalities have been developed and prototypically evaluated [18]. With a large number of controllable devices and complex network properties, the implementation in SDN is a complex process [19]. Cyber-physical co-simulation (CPCS) is one of the options to implement real-time implementation in SDN [20].

The use of cyber-physical real-time co-simulation that illustrates the complex behaviour of SDNs has gained attention in recent years [21]. The development of cyber-physical real-time co-simulation depends on the task for which they are designed [22]. The technical literature related to CPCS for SDN reviewed so far focuses mainly on cyber security, cyber theft detection [23], and false data detection [24]. Similarly, some of them use the cyber-physical real-time test only in a small system, for example a single converter system [25], without taking into account the dynamics of the DN. Only a few studies have focused on using the cyber-physical system for real-time RPC. For example, in [26], a distribution grid model was developed, implemented and simulated using OPAL-RT for dynamic performance evaluations in the real-time simulator (RTS). Similarly, in [27], three-phase electromechanical models for grid-following and grid-forming inverters were implemented in a three-phase DN. However, these articles do not consider the optimal OPF-based RPC in their studies. In [28], an attempt is proposed to realize real-time volt-watt control in a smart inverter considering voltage deviation as an objective function. However, this method incorporates offline optimization to obtain the optimal set points for smart inverters. Comprehensive studies of smart grid control functions are proposed on globally available power system networks using a RTS in [29]. The OPF is also implemented to obtain the optimal setpoints for SCs. But modelling of the converters and their real-time control is not implemented.

Considering the real-time operation of SDN for optimal RPC using the cyber-physical system, multiple converters, and the complex network property of SDN need to be considered. In addition, to operate the SDN optimally, real-time optimization is also another key factor that cannot be neglected. This paper presents a novel attempt to incorporate existing gaps as discussed above. Therefore, this paper proposes an OPF-based optimal RPC in SDN using CPCS. This paper uses the CPCS frameworks with multiple SCs, the converter controller, and the three-phase unbalanced DN to represent the realistic scenario of SDN. Furthermore, real-time optimization is also implemented in the paper to operate the SDN optimally. Therefore, the contribution made in this paper opens the multidimensional horizon for optimal real-time control and monitoring studies in SDN. In this paper, the focus is given on real-time OPF-based

RPC, but the CPCS framework developed during this study can also be utilized for many other DER integration studies in SDN. This paper proposes and validates the OPF-based RPC in SDN using CPCS. The main contributions made by the authors in this paper are listed below.

1. Develop a framework for an optimal OPF-based RPC using CPCS. The proposed framework is developed using real-time co-simulation between the distribution network solver (DNS) and RTS.
2. Design a controller for SCs in the physical layer (PL) of the cyber-physical framework and create a suitable monitoring and signal processing system to communicate with the optimal RPC centre. In addition, the proposed CPCS framework requires only a little information to update the system states of the designed controller and the SDN.
3. Develop a co-simulation-based optimization framework for obtaining the optimal reactive power setpoints to mitigate the voltage violations in the SDN. The performance of the co-simulation-based optimization is compared with several approaches before selecting the suitable algorithm and DNS.
4. The efficacy of the proposed OPF-based RPC using a real-time CPCS framework is validated by different scenarios of voltage violations created by changing the generation of power from DER and load consumption in real time. The proposed method can handle voltage violations using multiple SCs in the SDN.

The remainder of the paper is organized as follows. Section 2 covers the general method for real-time RPC using CPCS. The mathematical formulation of OPF-based RPC and co-simulation-based optimization is explained in Section 3. Similarly, the modelling of the SC is described in Section 4. The real-time simulation results and discussions are highlighted in Section 5. Finally, the last section concludes the main contribution and suggests future research directions. Further, test data information is included in Appendices.

2 | PROPOSED METHODOLOGY FOR OPF-BASED RPC IN SDN USING CYBER-PHYSICAL CO-SIMULATION

An overall method to implement the proposed OPF-based RPC in the SDN using CPCS is shown in Figure 1. Optimal RPC requires several important components for modelling, monitoring, controlling, and optimizing [2]. To achieve the general goals, two main components are necessary [30]. The first is the cybernetic layer (CL), which has major subcomponents like DNS, the Supervisory Control and Data Acquisition (SCADA) system, and the OPF-based RPC centre. The CL consists of tools and software to perform communication between the components within the CL and the PL. The CL is housed on the host PC that has related proprietary software and applications to manage the real-time digital simulator (RTS). The CL also has a user-defined SCADA panel, an OPF-based control centre, and a distribution system simulator. Furthermore, signal process-
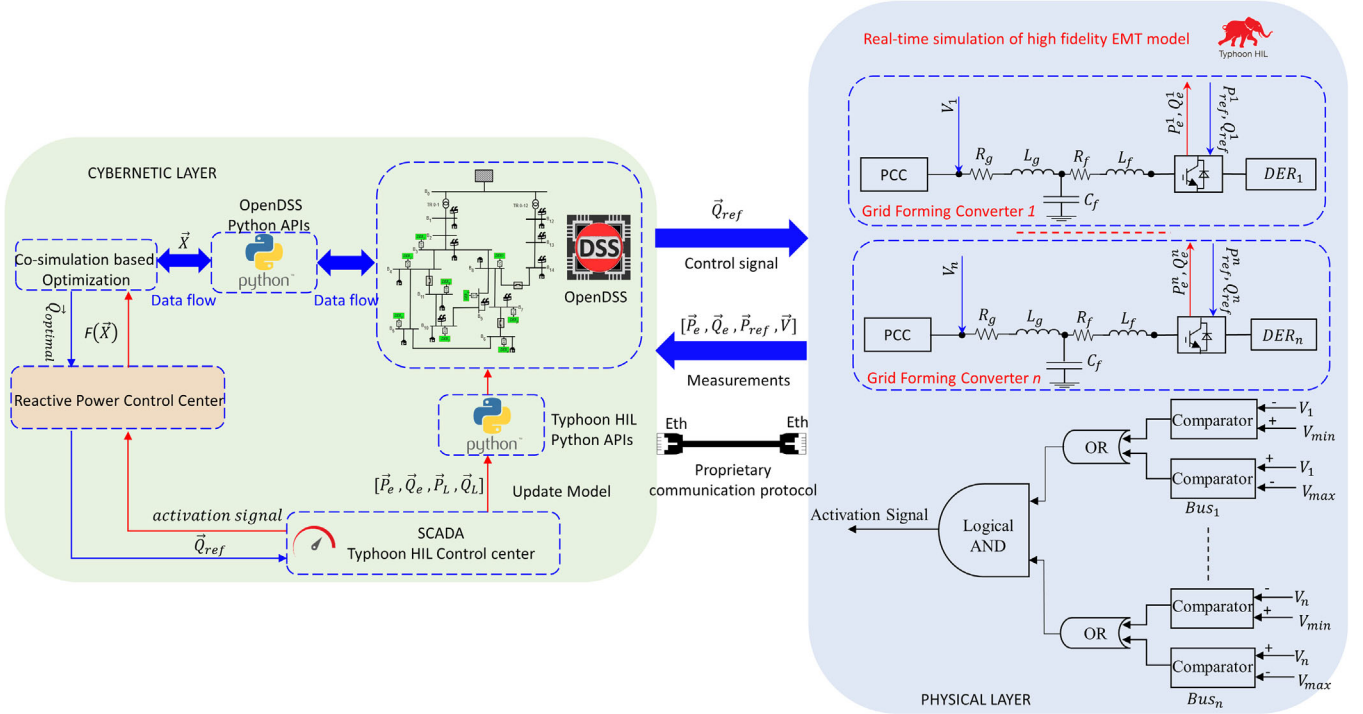
FIGURE 1 Overall method for OPF-based optimal RPC in SDN using proposed real-time cyber-physical co-simulation framework. OPF, optimal power flow; RPC, reactive power control; SDN, smart distribution network.

ing components and Python-based application programming interfaces (APIs) are present in the CL to operate in coordination with the model-based system engineering toolchain of DNS and RTS. The proposed CL also performs the OPF-based optimization as described in Section 3 to obtain the optimal reactive power set points for SCs. The CL also includes various graphical user interfaces (GUI) to interact with the PL and graphical displays to show the real-time output profile of the SDN. The PL is the other part where the real-time simulation of the SCs takes place. In PL, SCs with the controller as explained in Section 4 are designed. The monitoring system with signal processing components to detect the voltage violations is also present in the PL.

The active power references $\vec{P}_{ref}$ are created using the SCADA system in the CL. $\vec{Q}_{ref}$ is the optimal reactive power setpoints obtained from the OPF-based RPC centre. These $\vec{Q}_{ref}$ are sent from CL to PL using ethernet communication between CL and PL. The voltage reference on the nodes of the test system $\vec{V}$ is also exchanged to keep the same voltage profile of the point of common coupling (PCC) in both layers. The SC tracks the active power reference and the reactive power reference and provides the electrical power outputs $\vec{P}_e$ and $\vec{Q}_e$. In the PL, the activation signal generator block is also created. The OPF-based optimization is activated based on the activation signal obtained from the PL. A combination of logical *OR* and *AND* is utilized so that the activation signal is activated when voltage violations occur in the network. The control logic for a comparator used in the activation signal generator block is given by Equation (1). $|V_{IN}|$ is the bus voltage of the network and $|V_{REF}|$ is the ref-

erence voltage that can be according to the voltage regulation standard considered in the analysis. $|V_{OUT}|$ is the signal output of the comparator. Once the CL receives the information from the PL, the SCADA updates the system parameters of the SDN in the CL. The detailed methodology for running co-simulation between SCADA and the DNS in CL is presented in [31]

$$|V_{OUT}| = \begin{cases} 1, & |V_{IN}| > |V_{REF}| \\ 0, & |V_{IN}| < |V_{REF}| \\ no\ change, & |V_{IN}| = |V_{REF}| \end{cases} \quad (1)$$

The PL and CL are designed in the RTS and Typhoon hardware in loop (HIL) control centre of the RTS, respectively. The CL and the PL are connected using a proprietary Typhoon HIL communication protocol using an ethernet cable. $\vec{P}_e, \vec{Q}_e, \vec{P}_{ref}, \vec{Q}_{ref}, \vec{V}$ are the signals that are exchanged between the cybernetic and the PL to achieve the proposed real-time CPCS. Since OpenDSS is a powerful DNS [32] and Typhoon HIL is the latest technology for real-time applications [33]. In this paper, OpenDSS is considered as DNS and Typhoon HIL real-time simulator is RTS. The overall process is repeated until the user stops the user.

3 | OPTIMAL RPC IN SMART DISTRIBUTION NETWORK

The SC injects or absorbs reactive power to adjust the voltage profile of the SDN [34]. The absorption or injection of

reactive power has a considerable impact on power loss, as the R/X of the line in the DN is high. R is the resistance and X is the reactance of the interconnecting lines. Therefore, when reactive power is required, the impact of network power loss should be considered. This makes the RPC an optimization problem. There are various approaches to optimal control of reactive power in the scientific literature [35]. Most research shows that RPC can be decentralized, distributed, and centralized. The decentralized technique uses local measurements to determine the optimal settings for reactive power dispatch. On the other hand, the distributed method coordinates between the local controller and the central controller. The centralized method is an OPF-based method. OPF can be implemented in DNs with significant integration of DERs.

To implement the OPF-based method in the DN, the DN is typically modelled using the LinDistFlow equations [36] or sensitivity-based modelling [37] in the literature. All network features may not be represented by the linearized version of the DN. Further, the extensive mathematical model of the DN and convergence concerns are additional hurdles in real-time optimization of DNs. Modelling the network in the distribution system simulator and optimizing it through co-simulation [38] is one way to avoid explicit mathematical modelling of the SDN in the optimization model. This method also eliminates convergence concerns because the complicated power flow equations are solved in the co-simulation. This technique can also solve any form of network, whether balanced or unbalanced, radial or mesh, and single-phase or poly-phase. Hence, this paper presents co-simulation-based optimization to grab the advantages of co-simulation-based optimization in real-time applications.

To optimize the SDN using co-simulation. First, the model is built using DNS inside the host PC. The load and generation data from the DERs are defined in DNS. During co-simulation-based optimization, the DNS solves the load flow solutions. The optimization model is built separately using Python-based DNS APIs. Data exchange is implemented in Python so that the simulation runs in engine mode. The optimization model involves objective functions, constraints, and a suitable solver. In particular, the objective function considered in this co-simulation-based optimization is an explicit objective function obtained from co-simulation. In this paper, the objective function $F(\vec{x}, \vec{u})$ is formulated by using the exterior penalty function (EPF) method [39]. The arbitrary penalty function is used to transform constrained problems into unconstrained problems. The EPF is used to incorporate bus voltages ($\forall i = 1, 2, \ldots, N_{bus}$) constraints in the objective function and change it to an unconstrained objective function. N_{bus} is the number of buses in the test system. The objective function $F(\vec{x}, \vec{u})$ in Equation (2) is the linear combination of $f(\vec{x})$ and the penalty function $g(\vec{x}, \vec{u})$.

$$\min_{\vec{x}} F(\vec{x}, \vec{u}) = f(\vec{x}) + g(\vec{x}, \vec{u}) \quad (2)$$

The main aim is to find the reactive power setpoints for the DERs. The controllable variable $\vec{x}$ in Equation (3) is the vector of the reactive power from N_{DER} number of SCs available in the SDN.

$$\vec{x} = [Q_{DER_1} \cdots Q_{DER_j} \cdots Q_{DER_N}]^T \quad (3)$$

The reactive power output of DER is limited by its maximum apparent power and active power. Mathematically, Equation (4) is the available reactive power (Q_{DER_j}) from the SC of size (S_{DER_j}) that produces the active power of (P_{DER_j})

$$QDER_j \leq \pm\sqrt{|SDER_j|^2 - PDER_j^2} \; \forall \; j = 1, \ldots, N_{DER} \quad (4)$$

Furthermore, according to the IEEE 1547–2018 standard [40], the reactive power of SCs is limited, adding one more constraint to the optimization model as given by Equation (5).

$$-K \, SDER_j \leq QDER_j \leq K \times SDER_j \quad (5)$$

where K = scaling factor for reactive power limit and $j = 1, \ldots, N_{DER}$. The function $f(\vec{x})$ considered in this study is an explicit function obtained from the co-simulation and is given by Equation (6).

$$f(\vec{x}) = P_{loss}(\vec{x}) \quad (6)$$

The second part of the objective function is defined as an arbitrary penalty function $g(\vec{x}, \vec{u})$. The voltage limit for voltage is taken as (V^{min}, V^{max}). Many standards define the permissible voltage limits in the DN. In this scenario, however, the voltage limit is within (V^{min}) and (V^{max}). The penalty function is defined as Equation (7) [39].

$$g(\vec{x}, \vec{u}) = K_p \left[\sum_{j=1}^{N_{bus}} M_j(\vec{x}) \right] \quad (7)$$

where K_p is the penalty multiplier, an extremely high value that makes the objective function extremely high when the voltage violation occurs during the optimization process. In this paper, the penalty multiplier is taken with fixed value and is considered as K_p. The penalization functions $M_j(\vec{x})$ are defined by Equation (8)

$$M_j(\vec{x}) = \begin{cases} 0, & V_j^{min} \leq |V_j| \leq V_j^{max} \\ 1, & otherwise \end{cases} \forall \; j = 1, 2, \ldots N_{bus} \quad (8)$$

Equation (2) is the objective function of the problem and Equations (4) and (5) are the constraints for optimization.

The developed optimization model is solved using differential evolution (DE) algorithm. The flow chart of DE algorithm [41] is shown in Figure 2. Since DE is a population-based optimization algorithm, population size, and other parameters such as strategy, mutation, recombination index, seed, polish, tolerance, number of workers, and maximum iteration are
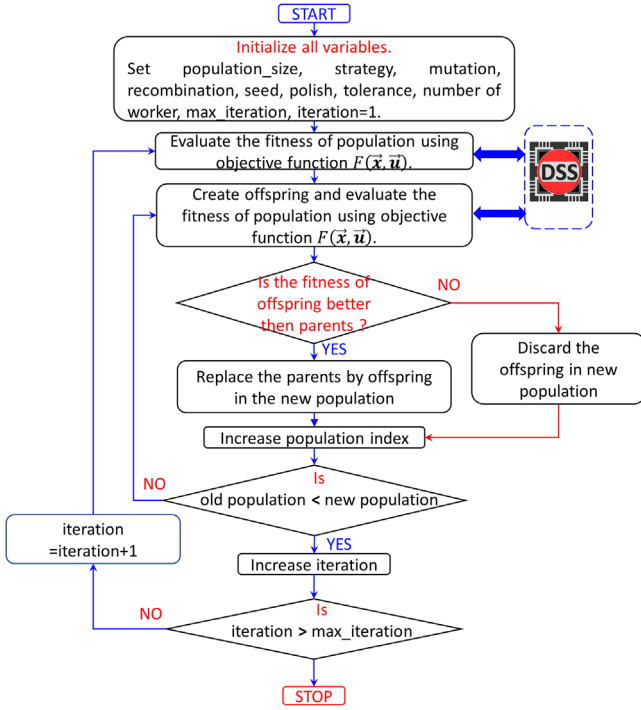
FIGURE 2 Flow chart for the differential evolution optimization algorithm [42]. maxiter = 1000, popsize = 15, tol = 0.01, mutation = (0.5, 1), recombination = 0.7, seed = None, callback = None, disp = False, polish = True, atol = 0, updating = immediate, workers = 1, x0 = None.

initialized in the initial phase. Once initialization is complete, the fitness function of the population is calculated using the objective function. From the population, offspring are generated, and the fitness functions for the offspring are also computed. If the fitness of the offspring is better than that of the parents, then the parent population is replaced by the offspring to find the best match. This process is repeated for all the populations until the maximum iteration is reached. The following parameters were considered for the DE algorithm. Strategy = best1bin,

4 | DETAILED MODELLING OF SMART CONVERTER

The power generated by renewable energy-based DERs, such as wind power plants and solar PV, fluctuates in nature or is different in nature (AC or DC), so its powers are not directly connected to the grid. In most cases, power electronics converters (PECs) are used. The PECs can be controlled and optimized to obtain regulated power output from the converters. Depending on the objective, the control algorithms are expected to set active power and reactive power set points for the converters. Many control strategies have been proposed in the literature [43]. Additionally, one of the deciding factors when selecting the appropriate control strategies is to consider the level of integration of DERs in the network. When a smaller number of DERs are present in the network, synchronous generators (SGs) in the

network can handle uncertain power dynamics. However, with increasing integration of DER, SGs will no longer be able to handle such system dynamics and maintain the system stability [44]. As converter-based DERs do not have spinning inertia or damping, the power system becomes more susceptible to instability [45]. The concept of virtual synchronous machines (VSM) [25] is gaining popularity among researchers to solve this problem. VSMs are physically PECs but synchronous machines mathematically. VSMs can supply virtual inertia and damping to the grid [46]. The synchronverter is one of the popular types of VSM [32]. So, in this paper, the synchronverter developed in [33] as a voltage source converter is used for real-time RPC.

The control of the synchronverters to regulate active and reactive power is governed by a mathematical model of the SG [49]. Assume that the stator windings are positioned in slots around the uniform air gap in a SC and that the stator winding has a self-inductance of L, mutual inductances of M, and resistances R_s characterize the stator winding. The electromagnetic flux ($\vec{\Phi}$) produced by the stator winding and the current ($\vec{I}$) flowing though winding can be represented by the equation Equation (9) [49]

$$\vec{\Phi} = \begin{bmatrix} \Phi_a \\ \Phi_b \\ \Phi_c \end{bmatrix}, \ \vec{I} = \begin{bmatrix} I_a \\ I_b \\ I_c \end{bmatrix} \quad (9)$$

The phase shift between the phases differs by $\frac{2\pi}{3}$. So, the phase shift vectors $\widetilde{cos}\theta$ and $\widetilde{sin}\theta$ are represented by Equation (10) [49]. θ_a is the rotor angle corresponding to phase a of VSM. For all three phases $\vec{\theta} = \begin{bmatrix} \theta_a \ \theta_b \ \theta_c \end{bmatrix}^T$

$$
\begin{aligned}
\widetilde{cos}\theta &= \begin{bmatrix} cos\theta_a \\ cos\theta_b \\ cos\theta_c \end{bmatrix} = \begin{bmatrix} cos\theta_a \\ cos\left(\theta_a - \frac{2\pi}{3}\right) \\ cos\left(\theta_a - \frac{4\pi}{3}\right) \end{bmatrix} \\
\widetilde{sin}\theta &= \begin{bmatrix} sin\theta_a \\ sin\theta_b \\ sin\theta_c \end{bmatrix} = \begin{bmatrix} sin\theta_a \\ sin\left(\theta_a - \frac{2\pi}{3}\right) \\ sin\left(\theta_a - \frac{4\pi}{3}\right) \end{bmatrix}
\end{aligned}
\quad (10)
$$

The phase terminal voltage $\vec{v} = \begin{bmatrix} v_a \ v_b \ v_c \end{bmatrix}^T$ of the generator is given by Kirchhoff's voltage law and can be represented by Equation (11) [49].

$$\vec{v} = \vec{e} - \begin{bmatrix} R_s \end{bmatrix} \vec{I} - \begin{bmatrix} L_s \end{bmatrix} \frac{d\vec{I}}{dt} \quad (11)$$

where $L_s = L + M$ and $\vec{e} = \begin{bmatrix} e_a \ e_b \ e_c \end{bmatrix}^T$ is the back emf. The back emf is given by Equation (13) [49] and $[R_s]$ and $[L_s]$ are

given by Equation (12).

$$[R_s] = \begin{bmatrix} R_s & 0 & 0 \\ 0 & R_s & 0 \\ 0 & 0 & R_s \end{bmatrix}$$

$$[L_s] = \begin{bmatrix} L_s & 0 & 0 \\ 0 & L_s & 0 \\ 0 & 0 & L_s \end{bmatrix} \tag{12}$$

$$\vec{e} = M_f I_f \dot{\theta} \widetilde{sin}\theta - M_f \frac{dI_f}{dt} \widetilde{cos}\theta \tag{13}$$

The relative location of the rotor axis and the magnetic field axis in a SG is fixed under normal operating conditions. However, any disturbance causes the rotor to decelerate or accelerate, reducing or increasing the rotor angle $\vec{\theta}$. The swing equation describes the relative motion of the rotor for a synchronously rotating air gap. The swing equation is given by Equation (14) [50].

$$\ddot{\theta} = \frac{1}{J}\left(T_m - T_e - D\dot{\theta}\right) \tag{14}$$

where J is the moment of inertia of the rotating parts, D is the damping factor, T_m is the vector of mechanical torque, and T_e is electromagnetic torque of VSM. The electromagnetic torque is given by Equation (15) [50].

$$T_e = M_f I_f \vec{I}, \widetilde{sin}\theta \tag{15}$$

where , denotes the inner product in $\mathbb{R}^3$.

The active and reactive power output of the SCs is obtained using Equation (16) [50].

$$P_e = \dot{\theta} M_f I_f \langle \vec{I}, \widetilde{sin}\theta \rangle$$
$$Q_e = -\dot{\theta} M_f I_f \langle \vec{I}, \widetilde{cos}\theta \rangle \tag{16}$$

The detailed design of the controller is more dependent on the application of the converter in the power system. This research aims to implement real-time RPC in the DN with a greater focus on network dynamics. Hence, this analysis does not consider a rotor-side controller (for maximum power tracking) to maintain the DC link voltage. Instead, for simplicity, a constant DC link voltage is considered. Only the grid-side controller to regulate active and reactive power is considered.

The overall block diagram for controlling active and reactive power using a synchronverter is explained in Figure 1. The $\vec{P}_{ref}$ and $\vec{Q}_{ref}$ are sent to the controller developed in the RTS schematic. The $\vec{P}_{ref}$ and $\vec{Q}_{ref}$ are the active power reference and reactive power reference for all the DERs in the SDN.
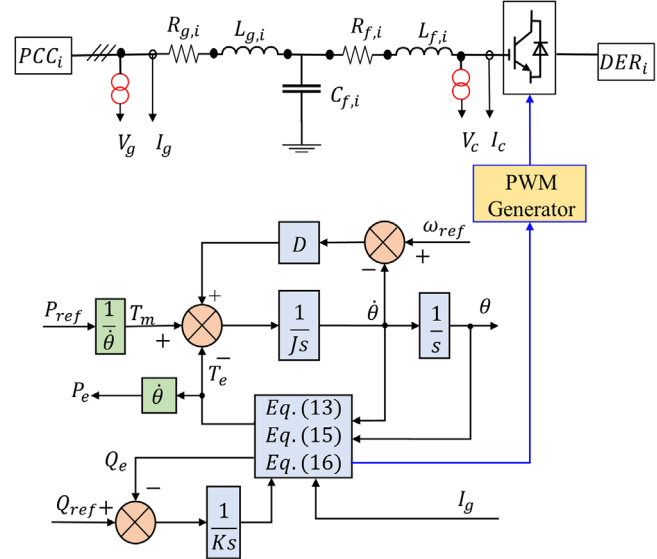

FIGURE 3 The control block diagram of the synchronverter [48].

$\vec{P}_{ref}$ and $\vec{Q}_{ref}$ for all the converters are considered as respectively in Equation (17)

$$\vec{P}_{ref} = [P_{ref,\,DER_1} \cdots P_{ref,\,DER_j} \cdots P_{ref,\,DER_N}]$$
$$\vec{Q}_{ref} = [Q_{ref,\,DER_1} \cdots Q_{ref,\,DER_j} \cdots Q_{ref,\,DER_N}] \tag{17}$$

The $\vec{Q}_{ref}$ are the reactive power obtained from the CL. Since the optimization is activated only when there is an activation signal, for other instances the $\vec{Q}_{ref}$ are kept the same as those values obtained from the previous optimization. The $\vec{Q}_{ref}$ are updated after the activation signal is triggered. Considering the losses in the controller and transformer system, the active power input to the converter $\vec{P}_{ref}$ is considered only 90%. So, the active power output $\vec{P}_e$ of the designed controller tracks $0.9\vec{P}_{ref}$. I_f is the vector of current flowing from the PCC of multiple inverters. ω_{ref} is the angular frequency which is a fixed value (314 rad/s for a 50 Hz system) in this study. The reference voltage reference of the grid $\vec{v}$ is set according to the voltage of the bus (where the SCs are connected) obtained from a real-time simulation. Equation (16) are the mathematical equations to obtain $\vec{P}_e$ and $\vec{Q}_e$. For multiple converters, $\vec{P}_e$ and $\vec{Q}_e$ are the active power and reactive power of all the converters and are given by Equation (18).

$$\vec{P}_e = [P_{e,\,DER_1} \cdots P_{e,\,DER_j} \cdots P_{e,\,DER_N}]$$
$$\vec{Q}_e = [Q_{e,\,DER_1} \cdots Q_{e,\,DER_j} \cdots Q_{e,\,DER_N}] \tag{18}$$

Figure 3 is the block diagram notation of Equations (8)–(16). The controller parameters considered in this study are given in Appendix 1. For simplicity, for this analysis, all the controllers are supposed to have the same parameters. Parameters are taken as proposed in [49].

5 | RESULTS AND DISCUSSIONS

This section illustrates the application of the proposed OPF-based optimal reactive power using CPCS. The research was carried out at the

Digital Energy Systems Laboratory (DIgEnSys-Lab). The DIgEnSys-Lab has physical equipment for real-time monitoring and control (https://fglongattlab.fglongatt.org). Typhoon HIL (HIL 604) is used as a RTS. Eight CPU cores, two digital I/O channels, and two analogue I/O channels are included in the HIL 604. Two advanced RISC machine (ARM) cores are also included. OpenDSS is considered as a DNS. The SDN is modelled in DNS, and the Python-based API is utilized to run the DNS in engine mode. Optimization is performed using a DE algorithm in SciPy [42]. A separate comparative study is performed to find the optimal optimization algorithm.

5.1 | Test system

In this paper, the CIGRE medium voltage (MV) DN is considered. The test system consists of two typical feeders at 20 kV, 50 Hz, and three-phase feeders 1 and 2. The feeder can be operated in radial or meshed topology by turning ON or OFF switch S1, S2, and S3. However, in this analysis, all switches are considered closed. Figure 4 shows an overview of the test system with GUI obtained during the real-time simulation. DERs are installed at the same location as suggested by the CIGRE benchmark. The size of DERs and loads is modified on the basis of sensitivity analysis. Appendix 2 and Appendix 3 are the rated size of the DERs and the load considered in this study.

5.2 | Sensitivity analysis of the test system

Before implementing the proposed method, a series of simulation studies were carried out. First, to observe the voltage profile of the network with the change in generation of power from DERs and loads, a sensitivity analysis is

performed. To perform the sensitivity analysis, a Monte Carlo simulation is done to obtain the voltage profile of the network random change in the generation of power from DERs and loads. Figures 5 and 6 are the voltage profiles of the monitored buses due to the change in power generation from DERs and loads at B_4, B_5, B_8, B_9, and B_{10} respectively. From the sensitivity analysis, it is observed that voltage violations can occur if the power generation from DERs is beyond some limits. Similarly, with the change in load, voltage violations occur if the loads are below and above certain limits.

5.3 | Simulation results without proposed method

First, simulation studies are performed without considering the proposed method. For this purpose, the load and generation profiles of the DERs are the same value as that considered for the real-time simulation studies. These values were stored using data loggers during the real-time simulation. Figure 7 is the voltage of the test system without implementing the proposed method. The V_{max} and V_{min} are are the upper and lower limits of the permissible phase voltage which is 5% above and below the rated phase voltage ($\frac{20}{\sqrt{3}}$ kV) of the test network. Voltage violations are observed when the proposed method is not implemented.

5.4 | Simulation with the proposed method

To verify the effectiveness of the proposed method, intentional voltage violations are created in the test system by changing the active power generation of the DERs and the loads at some buses. The power of the DERs and the loads can be changed in real time by changing the sliders in SCADA developed for this specific purpose. In this analysis, all DERs and only five loads at buses B_4, B_5, B_8, B_9, and B_{10} are changed in real time. The load is varied so that the voltage profile of the network varies above the prescribed limit. Figure 8 shows the load profile created during the real-time simulation. To plot all loads in the same figure, the load L_5 at B_{10} is scaled down by 10 times. The power generation from all DERs is changed during the real-time simulation.

The HIL OpenDSS co-simulation block continuously performs the load flow at each execution interval. The corresponding voltage profile is monitored through the monitoring system. When the voltage of any bus in the network exceeds the prescribed limit of 5% of the nominal phase voltage. The optimization block is activated as soon as the monitoring system senses some voltage violations; then the monitoring system makes the activation signal high. The activation signal for this case is shown in Figure 9. When the activation system is high, the OPF-based RPC centre activates the real-time co-simulation-based optimization block to perform the optimization. After completing optimization, first, the RPC centre exchanges the information with the SCADA. Later, SCADA updates the system states in the DN. At last, the CL sends the reactive power reference to the SC in the PL. The controller of the SCs tracks the electrical active and reactive power to the optimal reference value obtained from the CL. The electrical output from the SCs is fed to the DERs in the CL. SCADA updates the

model in DNS with values obtained from the PL. This process is repeated until the end of the simulation. The voltage profile of the DN using the proposed methodology is shown in Figure 10. In the figure, the voltage profile of only the node with DER integration is presented to make a clear visualization. The voltage profiles are within the prescribed limit.

Considering the limitation of the available RTS configuration in the lab, only four SCs are designed in RTS. For the rest of the DERs in the network, the active power reference and optimized reactive power are fed directly to the SDN. The physical converters developed in RTS are DER_1, DER_3, DER_6, and DER_9 connected to the buses at B_3, B_5, B_9, and B_7 respectively. However, the active power reference is changed for all DERs
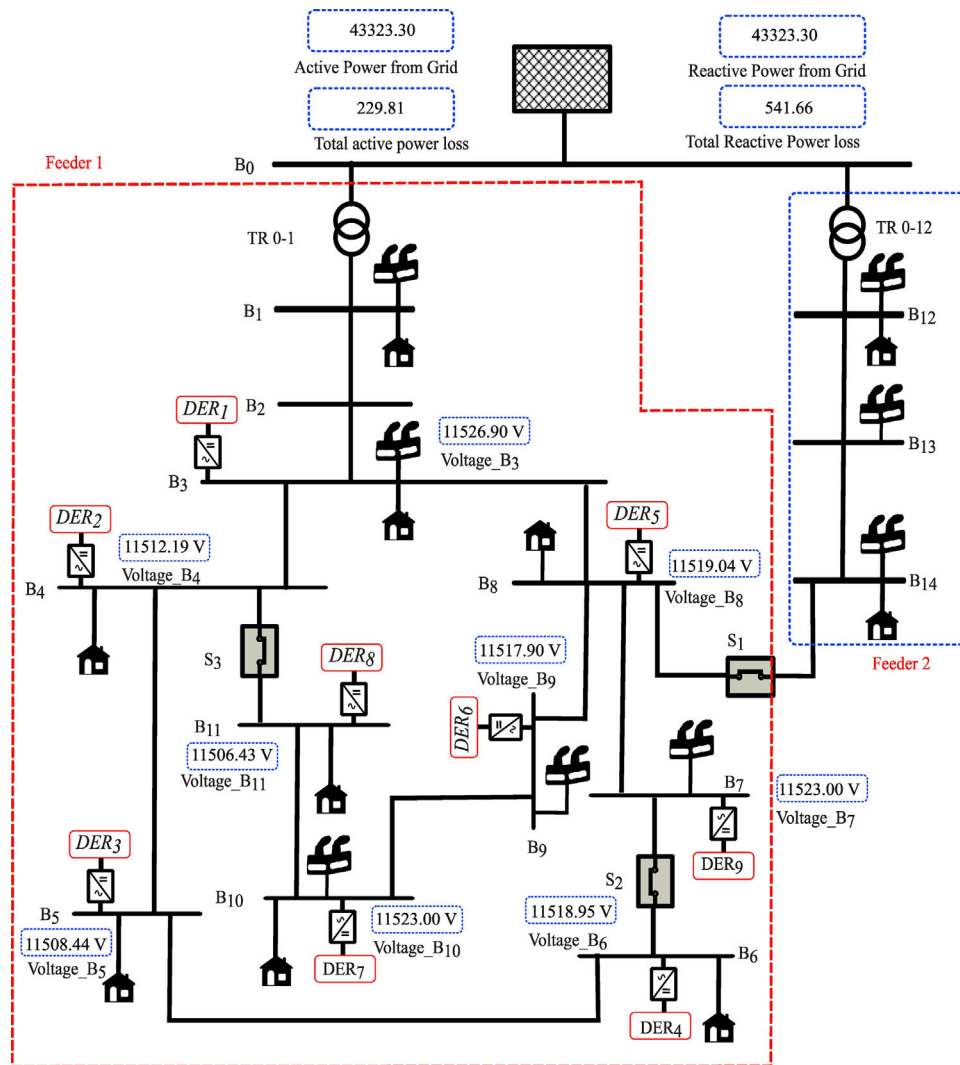
FIGURE 4　Modified layout of the CIGRE MV network with loads and DERs with GUI implemented in SCADA of the proposed CPCS [51]. CPCS, cyber-physical co-simulation; DERs, distributed energy resources; GUI, graphical user interfaces; MV, medium voltage; SCADA, supervisory control and data acquisition.
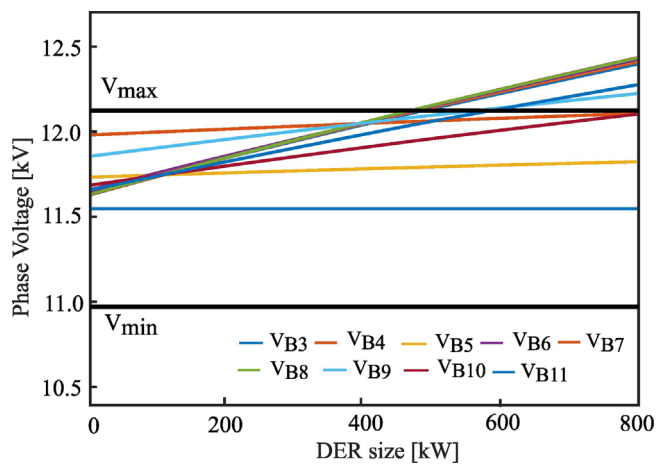

FIGURE 5　Voltage profile of the CIGRE MV network with change in size of all the DERs considered in this study. DERs, distributed energy resources; MV, medium voltage.
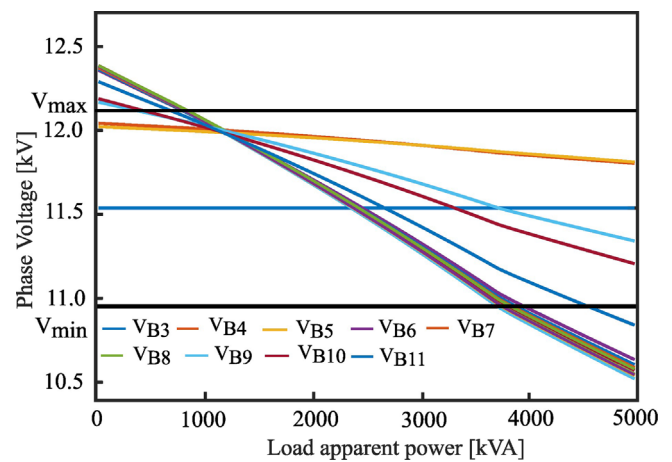

FIGURE 6　Voltage profile of the CIGRE MV network with change in load at B_4, B_5, B_8, B_9, and B_{10}. MV, medium voltage.
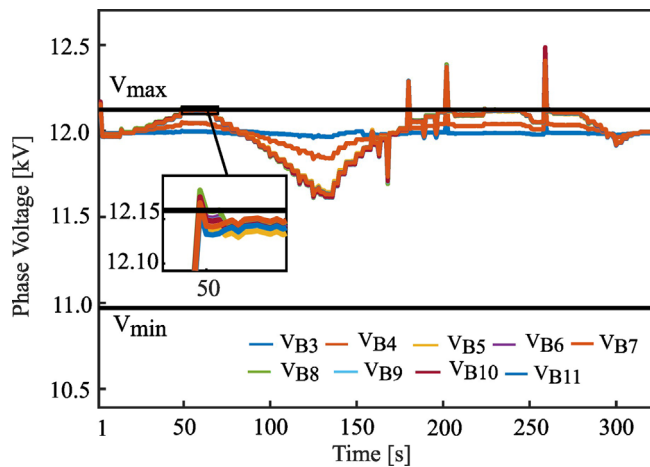
FIGURE 7 Voltage profile of the test system with the change in active power generations of DERs. This is obtained by simulation offline on the same test system without implementing the OPF-based RPC. DERs, distributed energy resources; OPF, optimal power flow; RPC, reactive power control.
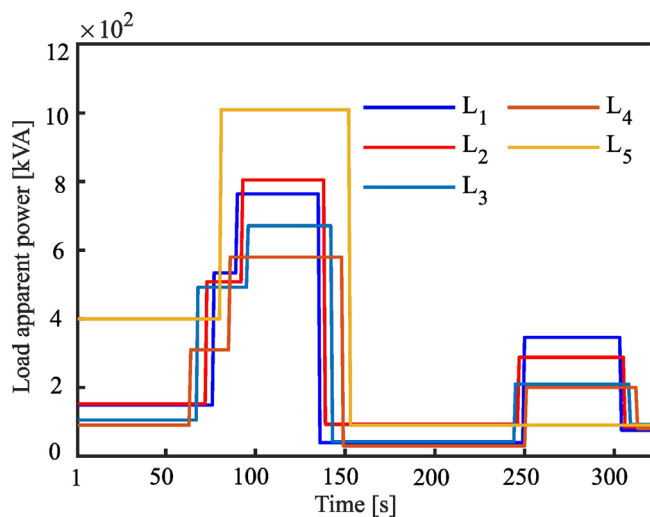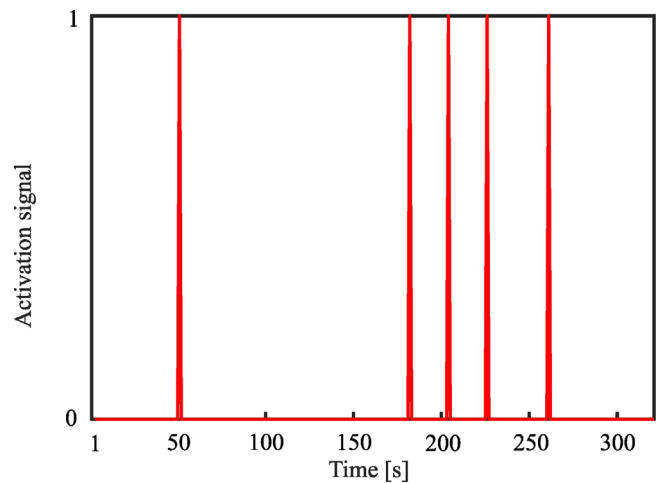

FIGURE 9 Activation signal from the monitoring system in the instances of voltage violations due to a change in the active power generation from DERs in real time. DER, distributed energy resources.
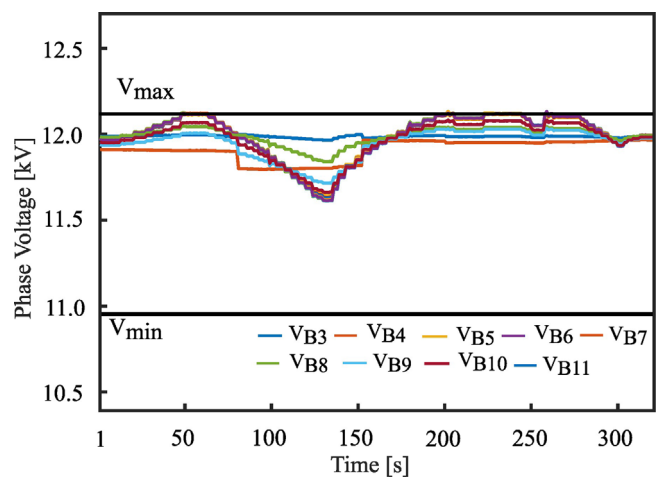

FIGURE 8 Load profile of the loads changed from SCADA in the cybernetic layer at B_4, B_5, B_8, B_9, and B_{10}. The load at B_4 is L_1, at B_5 is L_2, B_8 is L_3, B_9 is L_4, and at B_{10} is L_5. SCADA, supervisory control and data acquisition.

FIGURE 10 Voltage profile of the test system with proposed OPF-based RPC using cyber-physical co-simulation. OPF, optimal power flow; RPC, reactive power control.

TABLE 1 Computational performance of the proposed CPCS

Name of component	Number of utilized components	Utilized percentage
Standard processing core utilization	1 out of 3	33.33%
Signal generator utilization	12 out of 12	100%
Matrix memory utilization	–	0.50%
Simulation step time	1×10^{-6} (s)	–
Time slot utilization of core	–	62.25%
Signal processing IO variables utilization	38 out of 4,194,304	–
Signal processing probes utilization	52 out of 1024	5.07%
Total utilization of the internal memory	62 out of 254 kB	24.38%

CPCS, cyber-physical co-simulation.

connected in the network to change the real-time dynamics of the test system. Figure 11 shows the active power reference and the active power generated by the SCs.

During real-time simulation, to mitigate voltage violations, the proposed system performs real-time optimization to set the optimal reactive power references for each converter, as shown in Figure 12. These reactive power references are sent to the converters in the PL. The converter generates the reactive power to match the reference. With the reactive power generated by the converter, voltage violations were mitigated in the network.

Table 1 shows the computational performance of the proposed real-time system. From the table, it is observed that the proposed method can operate with a simulation time of 1×10^{-6} (s), total utilization of internal memory of 24.38% and
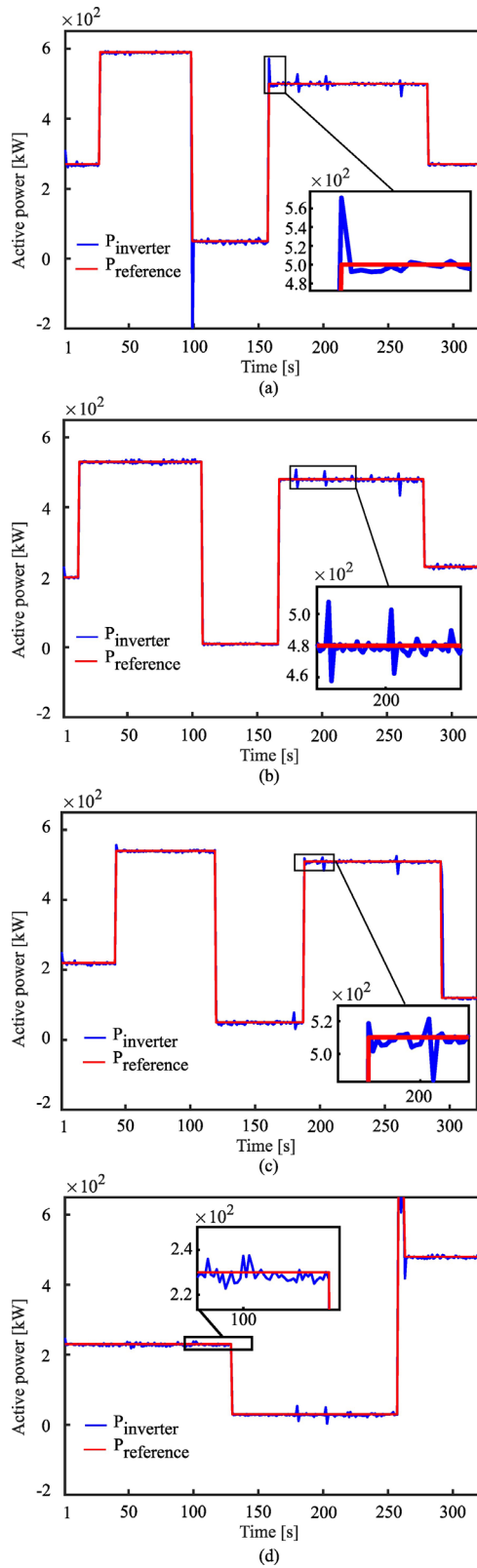
FIGURE 11 Active power references changed from SCADA in the cybernetic layer and electrical power output from smart converters obtained from the physical layer (a) DER_1 at B_3, (b) DER_3 at B_5, (c) DER_6 at B_9, and (d) DER_9 at B_7. DER, distributed energy resources; SCADA, supervisory control and data acquisition.
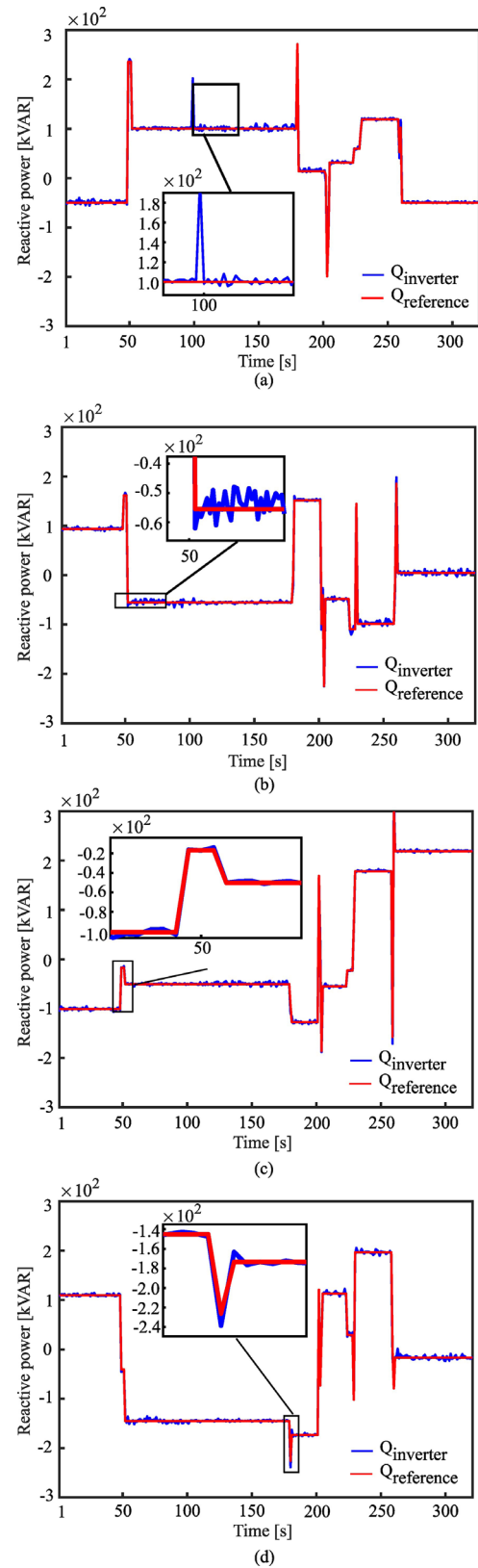
FIGURE 12 Reactive power references obtained from the OPF-based RPC centre and reactive power output from smart converters obtained from the physical layer (a) DER_1 at B_3, (b) DER_3 at B_5, (c) DER_6 at B_9, and (d) DER_9 at B_7. DER, distributed energy resources; OPF, optimal power flow; RPC, reactive power control.
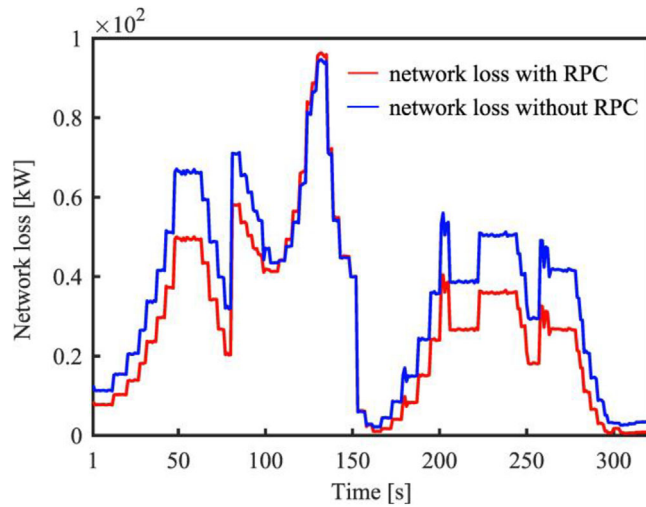
FIGURE 13 Comparison of the total system loss of the CIGRE MV network with the proposed real-time OPF-based reactive power control and without reactive power control. MV, medium voltage; OPF, optimal power flow.

by utilizing only 5.07% of available signal processing probes. All these performance parameters suggest that the proposed method is fast and computationally simple.

5.5 | Comparison of total system loss

The absorption or injection of reactive power has a considerable impact on total system loss in the DN. A comparison of system loss in the network with and without the proposed method is presented in Figure 13. The system loss is computed considering the same DER generation profiles, and the same load profiles considered for real-time studies. Since the optimization process obtains the optimal reactive power setpoints to reduce system loss, the network experiences lower losses with the proposed method. From the figure, it is also observed that the system loss over a period change in the network depends on the size of DER generation profile, size of load profile, and the reactive power support from the DERs.

6 | CONCLUSION AND OUTLOOK

With the advancement of SC information and communication capability, the use of SCs in real-time monitoring and control of the DN is increasing. Deployment of CPCS for real-time control and monitoring of realistic distribution with multiple controllable devices is still a big challenge. This research expands the multidimensional horizon for real-time control and monitoring studies. This research proposes a novel way of regulating the reactive power of SCs in SDNs using OPF-based optimal RPC on a proposed real-time CPCS framework. Real-time simulation studies show that the voltage profile of the DN can be regulated using the proposed methodology. This approach is simple and can be implemented on any type of network: single-phase or multiphase, balanced or unbalanced, and radial or mesh. The proposed framework is also capable of performing real-time CPCS studies with multiple numbers of controllable devices in the network.

The proposed CPCS framework can be implemented in several ways to test, develop, and validate the smart grid paradigm in the DN. Investigation with more advanced features of the smart grid is planned in the future.

NOMENCLATURE

$\vec{P}_e$	active power outputs of N_{DER} number of SC
$\vec{P}_{ref}$	active power references of N_{DER} number of VSM
$\vec{Q}_e$	reactive power outputs of N_{DER} number of SC
$\vec{Q}_{ref}$	reactive power references of N_{DER} number of SC
$|V_{IN}|$	input bus voltage of the network to comparator
$|V_{OUT}|$	signal output of the comparator
$|V_{REF}|$	reference bus voltage for the comparator
K_p	penalty multiplier (1000)
K_v	reactive power droops of VSM
N_{DER}	number of DERs in the SDN
N_{bus}	number of buses on the SDN
P_{DER_j}	active power of DER at node j
Q_{DER_j}	reactive power of DER at node j
S_{DER_j}	apparent power of DER at node j
T_e	electromagnetic torques of VSM
T_m	mechanical torques of VSM
V_j^{min}	lower limit of voltage at node j
$\vec{v}$	voltage at the nodes of the test system
v_j^{max}	upper limit of voltage at node j
ω_{ref}	reference angular speed (rad/s)
AND	logical AND
API	application programming interface
CL	cybernetic layer
CPCS	cyber-physical co-simulation
DE	differential evolution
DER	distributed energy resources
DN	distribution network
DNS	distribution network solver
HIL	hardware in loop
IED	intelligent electronics devices
MV	medium voltage
OPF	optimal power flow
OR	logical OR
PCC	point of common coupling
PEC	power electronics converter
PL	physical layer
R	resistance of the interconnecting lines
RPC	reactive power control
RTS	real-time simulator
SC	smart converters
SCADA	supervisory control and data acquisition
SDN	smart distribution network
SG	synchronous generator
VSM	virtual synchronous machine
X	reactance of the interconnecting lines

D damping constant of VSM

J moment of Inertia of VSM

K scaling factor for reactive power limit

AUTHOR CONTRIBUTIONS

ACKNOWLEDGEMENTS

CONFLICT OF INTERESTS STATEMENT

The authors declare that they have no competing interests.

DATA AVAILABILITY STATEMENT

The essential data are attached in the paper. All other source codes, executables, sample datasets, and documents are available on request from the corresponding author.

FUNDING INFORMATION

ORCID

Raju Wagle https://orcid.org/0000-0002-1880-3464
Mohammad Amin https://orcid.org/0000-0003-0391-9322

REFERENCES

1. Chen, S., Liu, P., Li, Z.: Low carbon transition pathway of power sector with high penetration of renewable energy. Renew. Sustain. Energy Rev. 130, 109985 (2020)
2. Borlase, S.: Smart Grids Infrastructure, Technology, and Solutions, 1st ed. CRC Press, Boca Raton, FL (2017)
3. Harirchi, F., Simoes, M.G.: Enhanced instantaneous power theory decomposition for power quality smart converter applications. IEEE Trans. Power Electron. 33(11), 9344–9359 (2018)
4. Acosta, M.N., Gonzalez-Longatt, F., Andrade, M.A., Torres, J.R.: Optimal reactive power control of smart inverters: Vestfold and telemark regional network. In: 2021 IEEE Madrid PowerTech, pp. 1–6 (2021)
5. Sinsel, S.R., Riemke, R.L., Hoffmann, V.H.: Challenges and solution technologies for the integration of variable renewable energy sources—A review. Renew. Energy 145, 2271–2285 (2020)
6. Tang, L., Han, Y., Yang, P., Wang, C., Zalhaf, A.S.: A review of voltage sag control measures and equipment in power systems. Energy Rep. 8, 207–216 (2022)
7. Bollen, M.H.J., Das, R., Djokic, S., Ciufo, P., Meyer, J., Ronnberg, S.K., Zavodam, F.: Power quality concerns in implementing smart distribution-grid applications. IEEE Trans. Smart Grid 8(1), 391–399 (2017)
8. Tofighi-Milani, M., Fattaheian-Dehkordi, S., Fotuhi-Firuzabad, M., Lehtonen, M.: Decentralized active power management in multi-agent distribution systems considering congestion issue. IEEE Trans. Smart Grid 13(5), 3582–3593 (2022)
9. Vergara, P.P., Salazar, M., Mai, T.T., Nguyen, P.H., Slootweg, H.: A comprehensive assessment of PV inverters operating with droop control for overvoltage mitigation in LV distribution networks. Renew. Energy 159, 172–183 (2020)
10. Fattaheian-Dehkordi, S., Abbaspour, A., Mazaheri, H., Fotuhi-Firuzabad, M., Lehtonen, M.: A new framework for mitigating voltage regulation issue in active distribution systems considering local responsive resources. IEEE Access 9, 152585–152594 (2021)
11. Fadlullah, Z.M., Fouda, M.M., Kato, N., Takeuchi, A., Iwasaki, N., Nozaki, Y.: Toward intelligent machine-to-machine communications in smart grid. IEEE Commun. Mag. 49(4), 60–65 (2011)
12. Guleryuz Halacli, M., Demiroren, A.: Techno-economic management of daily Volt/Var planning considering reactive power contribution of high penetrated-PV solar farms utilized as STATCOM: A case study in Istanbul, Turkey. Int. Trans. Electr. Energy Syst. 31(3), 1–24 (2021)
13. Chaudhary, P., Rizwan, M.: Voltage regulation mitigation techniques in distribution system with high PV penetration: A review. Renew. Sustain. Energy Rev. 82, 3279–3287 (2018)
14. Ceylan, O., Paudyal, S., Pisica, I.: Nodal sensitivity-based smart inverter control for voltage regulation in distribution feeder. IEEE J. Photovolt. 11(4), 1105–1113 (2021)
15. Nour, A.M.M., Hatata, A.Y., Helal, A.A., El-Saadawi, M.M.: Review on voltage-violation mitigation techniques of distribution networks with distributed rooftop PV systems. IET Gener. Transm. Distrib. 14(3), 349–361 (2020)
16. Zhao, E., Han, Y., Lin, X., Liu, E., Yang, P., Zalhaf, A.S.: Harmonic characteristics and control strategies of grid-connected photovoltaic inverters under weak grid conditions. Int. J. Electr. Power Energy Syst. 142(PB), 108280 (2022)
17. Han, Y., Feng, Y., Yang, P., Xu, L., Zalhaf, A.S.: An efficient algorithm for atomic decomposition of power quality disturbance signals using convolutional neural network. Electr. Power Syst. Res. 206, 107790 (2022)
18. Marot, A., Kelly, A., Naglic, M., Barbesant, V., Cremer, J., Stefanov, A., Viebahn, J.: Perspectives on future power system control centers for energy transition. J. Mod. Power Syst. Clean Energy 10(2), 328–344 (2022)
19. Tran, M.Q., Elsisi, M., Liu, M.-.K., Vu, V.Q., Mahmoud, K., Darwish, M.M.F., Abdelaziz, A.Y., Lehtonene, M.: Reliable deep learning and IoT-based monitoring system for secure computer numerical control machines against cyber-attacks with experimental verification. IEEE Access 10, 23186–23197 (2022)
20. Tramarin, F., Luvisotto, M., Willig, A., Yu, K.: Guest editorial: Industrial cyber-physical systems - new trends in computing and communications. IEEE Trans. Ind. Inform. 17(5), 3518–3522 (2021)
21. Yohanandhan, R.V., Elavarasan, R.M., Manoharan, P., Mihet-Popa, L.: Cyber-physical power system (CPPS): A review on modeling, simulation, and analysis with cyber security applications. IEEE Access 8, 151019–151064 (2020)
22. Elsisi, M., Tran, M.Q., Mahmoud, K., Mansour, D.E.A., Lehtonen, M., Darwish, M.M.F.: Towards secured online monitoring for digitalized GIS against cyber-attacks based on IoT and machine learning. IEEE Access 9, 78415–78427 (2021)
23. Khan, M.M.S., Giraldo, J.A., Parvania, M.: Attack detection in power distribution systems using a cyber-physical real-time reference model. IEEE Trans. Smart Grid 13(2), 1490–1499 (2022)
24. Badr, M.M., Ibrahem, M.I., Mahmoud, M., Fouda, M.M., Alsolami, F., Alasmary, W.: Detection of false-reading attacks in smart grid net-metering system. IEEE Internet Things J. 9(2), 1386–1401 (2022)

25. Milton, M., De La, C.O., Ginn, H.L., Benigni, A.: Controller-embeddable probabilistic real-time digital twins for power electronic converter diagnostics. IEEE Trans. Power Electron. 35(9), 9850–9864 (2020)

26. Hooshyar, H., Mahmood, F., Vanfretti, L., Baudette, M.: Specification, implementation, and hardware-in-the-loop real-time simulation of an active distribution grid. Sustain. Energy, Grids Netw. 3, 36–51 (2015)

27. Du, W., Tuffner, F.K., Schneider, K.P., Lasseter, R.H., Xi, J., Chen, Z., Bhattarai, B.: Modeling of grid-forming and grid-following inverters for dynamic simulation of large-scale distribution systems. IEEE Trans. Power Deliv. 36(4), 2035–2045 (2021)

28. Kashani, M.G., Mobarrez, M., Bhattacharya, S.: Smart inverter volt-watt control design in high PV-penetrated distribution systems. IEEE Trans. Ind. Appl. 55(2), 1147–1156 (2019)

29. Palaniappan, R., Molodchyk, O., Shariati-Sarcheshmeh, M., Asmah, M.W., Liu, J., Schlichtherle, T., Richter, F., Kwofie, E.A., Festner, D.R., Blanco, G., Mutule, A., Borscevskis, O., Rafaat, S.S., Li, Y., Häger, U., Rehtanz, C.: Experimental verification of smart grid control functions on international grids using a real-time simulator. IET Gener. Transm. Distrib. 16(13), 1–14 (2022)

30. Wagle, R., Tricarico, G., Sharma, P., Sharma, C., Reuda, J.L., Gonzalez-Longatt, F.: Cyber-physical co-simulation testbed for real-time reactive power control in smart distribution network. In: 2022 IEEE Innovative Smart Grid Technologies - Asia (ISGT ASIA) (2022)

31. Wagle, R., Sharma, P., Amin, M., Gonzalez-Longatt, F.: Cyber-physical co-simulation framework between typhon HIL and OpenDSS for real-time applications. In: Real-Time Simulation & Hardware-in-the-Loop Testing using Typhoon HIL (accepted chapter) (2022)

32. Gao, D.W., Muljadi, E., Tian, T., Miller, M.: Software comparison for renewable energy deployment in a distribution network. National Renewable Energy Lab.(NREL), Golden, CO (United States) (2017)

33. Gonzalez-Longatt, F.: Experiences in Digital Real-Time Simulation to achieve carbon neutrality. Sustainable Development and Recent Advances in Electrical Engineering (SDRAEE), (2022)

34. Pettersen, D., Melfald, E., Chowdhury, A., Acosta, M.N., Gonzalez-Longatt, F., Topic, D.: TSO-DSO performance considering volt-var control at smart-inverters: Case of vestfold and telemark in Norway. In: Proceedings of 2020 International Conference on Smart Systems and Technologoies SST 2020, vol. 1547(2018), pp. 147–152 (2020))

35. Mahmud, N., Zahedi, A.: Review of control strategies for voltage regulation of the smart distribution network with high penetration of renewable distributed generation. Renew. Sustain. Energy Rev. 64, 582–595 (2016)

36. Molina-García, Á., Mastromauro, R.A., García-Sánchez, T., Pugliese, S., Liserre, M., Stasi, S.: Reactive power flow control for PV inverters voltage support in LV distribution networks. IEEE Trans. Smart Grid 8(1), 447–456 (2017)

37. Kang, S.J., Kim, J., Park, J.W., Baek, S.M.: Reactive power management based on voltage sensitivity analysis of distribution system with high penetration of renewable energies. Energies 12(8), 1493 (2019)

38. Alvarado-Barrios, L., Álvarez-Arroyo, C., Escaño, J.M., Gonzalez-Longatt, F.M., Martinez-Ramos, J.L.: Two-level optimisation and control strategy for unbalanced active distribution systems management. IEEE Access 8, 197992–198009 (2020)

39. Krechel, T., Sanchez, F., Gonzalez-Longatt, F., Chamorro, H.R., Rueda, J.L.: A transmission system friendly micro-grid: Optimising active power losses. In: 2019 IEEE Milan PowerTech, pp. 1–6 (2019)

40. IEEE Standard for Interconnection and Interoperability of Distributed Energy Resources with Associated Electric Power Systems Interfaces–Amendment 1: To Provide More Flexibility for Adoption of Abnormal Operating Performance Category III. IEEE Std 1547a-2020 (Amendment to IEEE Std 1547–2018), pp. 1–16 (2020)

41. Storn, R., Price, K.: Differential evolution – A simple and efficient heuristic for global optimization over continuous spaces. J. Glob. Optim. 11(4), 341–359 (1997)

42. Virtanen, P., Gommers, R., Oliphant, T.E., Haberland, M., Reddy, T., Cournapeau, D., Burovski, E., Peterson, P., Weckesser, W., Bright, J., van der Walt, S.J., Brett, M., Wilson, J., Millman, K.J., Mayorov, N., Nelson, A.R.J., Jones, E., Kern, R., Larson, E., Carey, C.J., Polat, İ., Feng, Y., Moore, E.W., VanderPlas, J., Laxalde, D., Perktold, J., Cimrman, R., Henriksen, I.,

Quintero, E.A., Harris, C.R., Archibald, A.M., Ribeiro, A.H., Pedregosa, F., van Mulbregt, P.; SciPy 1.0 Contributors: SciPy 1.0: Fundamental algorithms for scientific computing in Python. Nat. Methods 17(3), 261–272 (2020)

43. Ansari, S., Chandel, A., Tariq, M.: A comprehensive review on power converters control and control strategies of AC/DC microgrid. IEEE Access 9, 17998–18015 (2021)

44. Tamrakar, U., Shrestha, D., Maharjan, M., Bhattarai, B.P., Hansen, T.M., Tonkoski, R.: Virtual inertia: Current trends and future directions. Appl. Sci. 7(7), 1–29 (2017)

45. Van Wesenbeeck, M.P.N., De Haan, S.W.H., Varela, P., Visscher, K.: Grid tied converter with virtual kinetic storage. In: 2009 IEEE Bucharest PowerTech Innov. Ideas Towar. Electr. Grid Futur. (1), 1–7 (2009)

46. Azuara-Grande, L.S., Gonzalez-Longatt, F., Tricarico, G., Wagle, R., Arnaltes, S., Granizo, R.: Real-time implementation of two grid-forming power converter controls to emulate synchronous generators. In: 2022 IEEE Biennial Congress of Argentina (ARGENCON), pp. 1–6 (2022)

47. Zhong, Q.C., Weiss, G.: Synchronverters: Inverters that mimic synchronous generators. IEEE Trans. Ind. Electron. 58(4), 1259–1267 (2011). https://doi.org/10.1109/TIE.2010.2048839

48. Zhong, Q.C.: Virtual synchronous machines: A unified interface for grid integration. IEEE Power Electron. Mag. 3(4), 18–27 (2016)

49. Zhong, Q.C., Ma, Z., Ming, W.L., Konstantopoulos, G.C.: Grid-friendly wind power systems based on the synchronverter technology. Energy Convers. Manag. 89, 719–726 (2015)

50. Grainger, W.D., Stevenson, J.J.: Power System Analysis. McGraw-Hill, New York (1994)

51. Cigre: Benchmark systems for network integration of renewable and distributed energy resources. 2014

APPENDIX
Appendix A

Parameters of the synchronverter [49]

Parameters	Value	Unit
Moment of inertia (J)	0.1	(kg/m^2)
Mechanical friction (D)	1	(N m s)
Reactive power droop (K_v)	0.0001	–
Angular speed (ω)	314	(rad/s)
Filter resistance (R)	0.1	Ω
Filter inductance (L)	10.1859	(mH)
Filter capacitance (C)	24	(μF)
$M_f \vec{I}_f$	$\begin{bmatrix} 0.5 & 0 & 0 \\ 0 & 0.5 & 0 \\ 0 & 0 & 0.5 \end{bmatrix}$	(V s)

Appendix B

Rating of the DERs considered in this study

| Name of DER | Rating of DERs | |
	P (kW)	Q (kVAr)
DER_1	690.00	303.00
DER_1	690.00	303.00
DER_1	680.00	300.00
DER_1	680.00	300.00
DER_1	740.00	325.00
DER_1	740.00	325.00
DER_1	740.00	325.00
DER_1	740.00	325.00
DER_1	740.00	325.00

Appendix C

Rating of residential and commercial loads considered in this study. These load profiles were taken at 19:00 [34]

| Bus | Apparent power, S [kVA] | | Power factor | |
	Residential	Industrial	Residential	Industrial
B_1	74.00	20.70	0.98	0.95
B_2	—	—	—	—
B_3	264.00	1.30	0.97	0.85
B_4	812.20	—	0.97	—
B_5	894.70	—	0.97	—
B_6	532.40	—	0.97	—
B_7	—	0.40	—	0.85
B_8	760.40	—	0.97	—
B_9	—	3.30	—	0.85
B_{10}	653.90	0.40	0.97	0.85
B_{11}	315.00	—	0.97	—
B_{12}	14172.90	25.50	0.98	0.95
B_{13}	—	0.20	—	0.85
B_{14}	199.20	1.90	0.97	0.85